Biophysical Journal
Article

Biophysical Society

The Effect of Temperature on Microtubule-Based Transport by Cytoplasmic Dynein and Kinesin-1 Motors

Weili Hong,[1] Anjneya Takshak,[3] Olaolu Osunbayo,[2] Ambarish Kunwar,[3] and Michael Vershinin[1,2,*]
[1]Department of Physics & Astronomy and [2]Department of Biology, University of Utah, Salt Lake City, Utah; and [3]Department of Biosciences and Bioengineering, Indian Institute of Technology Bombay, Powai, Mumbai, Maharashtra, India

ABSTRACT Cytoplasmic dynein and kinesin are both microtubule-based molecular motors but are structurally and evolutionarily unrelated. Under standard conditions, both move with comparable unloaded velocities toward either the microtubule minus (dynein) or plus (most kinesins) end. This similarity is important because it is often implicitly incorporated into models that examine the balance of cargo fluxes in cells and into models of the bidirectional motility of individual cargos. We examined whether this similarity is a robust feature, and specifically whether it persists across the biologically relevant temperature range. The velocity of mammalian cytoplasmic dynein, but not of mammalian kinesin-1, exhibited a break from simple Arrhenius behavior below 15°C—just above the restrictive temperature of mammalian fast axonal transport. In contrast, the velocity of yeast cytoplasmic dynein showed a break from Arrhenius behavior at a lower temperature (~8°C). Our studies implicate cytoplasmic dynein as a more thermally tunable motor and therefore a potential thermal regulator of microtubule-based transport. Our theoretical analysis further suggests that motor velocity changes can lead to qualitative changes in individual cargo motion and hence net intracellular cargo fluxes. We propose that temperature can potentially be used as a noninvasive probe of intracellular transport.

INTRODUCTION

Intracellular transport along microtubules (MTs) facilitates and maintains cellular order, and makes possible the existence of spatially extended cells such as neurons. In most cells, cargo transport operates in a variety of environmental conditions, including a wide range of temperatures. Even for mammals, this range can be as wide as 5–45°C for hibernating species (1). The temperature dependence of in vivo transport velocities has often been reported to be Arrhenius-like (2), but non-Arrhenius deviations, including cold block of transport below ~12°C, are also well established (2). The origin of this rich set of in vivo phenotypes is unclear.

Intracellular transport is often driven by small ensembles (n = ~2–6) of molecular motors (3,4). When opposite polarity motors are present in the same ensemble, the sign and magnitude of net cargo velocity reflect the balance of competitive or alternating mechanochemical activity of various motors (5–7). Thus, it is impossible to gain a quantitative understanding of temperature-dependent in vivo phenotypes without knowing the temperature dependence of the enzymatic activity of individual kinesin and dynein motors that drive transport. However, this aspect of motor function is poorly understood. Previous variable-temperature in vitro motility assays with kinesins (8–10) have been limited to a relatively narrow temperature window that roughly covers the survival range of most mammals. Broader ranges have been explored via biochemical methods (11,12), but not biophysical ones. Although published data on kinesin is somewhat limited, scant variable temperature data are available for cytoplasmic dynein. In this work, we aimed to address this gap in understanding by examining kinesin and cytoplasmic dynein motilities under controlled in vitro conditions, with identical environmental factors affecting motor activity.

We first used bead assays to examine how the velocities and force-production abilities of kinesin-1 and mammalian cytoplasmic dynein motors change with temperature. Measurements of velocity were prioritized over measurements of the motor enzymatic rate because mechanochemical coupling efficiency remains controversial for many motors (especially cytoplasmic dynein) even at the single-molecule

Submitted December 7, 2015, and accepted for publication August 2, 2016.
*Correspondence: vershinin@physics.utah.edu
Editor: Jennifer Ross.
http://dx.doi.org/10.1016/j.bpj.2016.08.006

level. We were surprised to find significant differences between kinesin and dynein motilities as a function of temperature. We use theoretical modeling to examine how our findings relate to motor ensemble performance, and further discuss the implications of our data for biological phenotypes and cell biology experiments.

MATERIALS AND METHODS

Motor purification

Mammalian cytoplasmic dynein was purified from rat brain as previously described (13). Full-length KIF5A heavy-chain dimers were expressed and purified as previously described (14). The minimal, GST-dimerized *Saccharomyces cerevisiae* dynein construct (15) (purified protein) was a generous gift from the lab of Dr. Ronald Vale.

In vitro motility assay

In vitro motility assays involving attachment of motor proteins to 1-μm-diameter polystyrene beads were performed as previously described (14). Motility and force production were determined using a 980 nm laser trap in accordance with previously described protocols (16) except that bead positions were recorded using a high-speed video camera (MQ003MG-CM; Ximea, Golden, CO) at 4000 fps and subsequently tracked using custom software (MATLAB, The MathWorks, Natick, MA). This approach was used to avoid condenser contact with the sample and thereby ensure better temperature uniformity and control. Note that the pKa shift of our PIPES-based buffers was negligible over the relevant temperature range.

For motility measurements, the optical trap was shut off as soon as bead binding to MTs was observed. Processivity was measured for bead binding fractions of 0.3 or below.

Temperature control

The full details of our setup differ from existing variable-temperature optical trapping setups (10,17–19) and will be described in detail elsewhere. Briefly, a customized Peltier thermoelectric stage (PE120; Linkam, Tadworth, UK) was used to control the slide temperature. A sapphire cover glass was used to maximize heat conductivity between the temperature control plate and the assay. We ensured good temperature contact by using a thin layer of water between the sapphire cover glass and the thermal stage. We also minimized heat sinking by eliminating condenser contact with the sapphire cover glass. To do so, we avoided using back focal plane interferometry to record and track bead positions, and instead used a high-speed camera (recording rate: 4000 fps) and custom video tracking software for this purpose. We calibrated the assay sample temperature with $\pm 0.5^{\circ}$C precision using several independent noncontact methods, including measuring bead diffusion (20–22), performing fixed-point calibration, and measuring the thermal shift of the peak of emission spectra for Cd-Se and Cd-Te quantum dot fluorescence (23). Further details of the temperature control and calibration will be published elsewhere.

Simulations

We used the stochastic model developed by Kunwar et al. (24,25) to simulate the temperature dependence of bidirectional cargo transport by multiple molecular motors of opposite types. The details of our model are further described in Supporting Materials and Methods in the Supporting Material.

RESULTS

We first examined the temperature dependence of the velocity of mammalian cytoplasmic dynein and mammalian kinesin-1 (Fig. 1). The velocities of beads driven by the kinesin-1 family member KIF5A and mammalian cytoplasmic

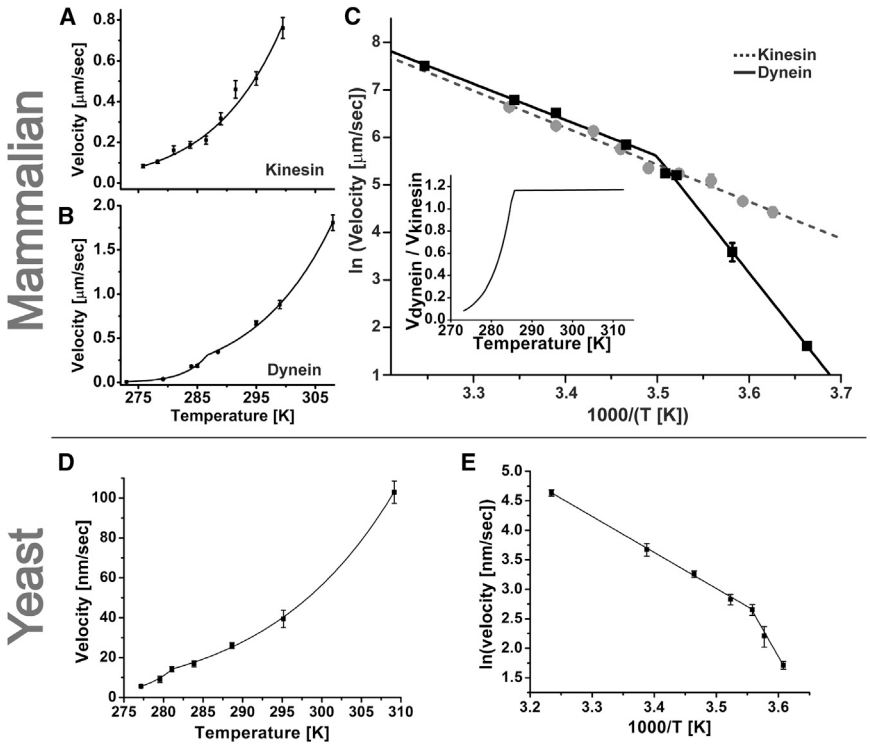

FIGURE 1 Temperature impacts the velocities of kinesin and mammalian cytoplasmic dynein differently. (*A*) Kinesin velocity and Arrhenius fit (*solid line*) down to 8°C. (*B*) Dynein velocity and fit to a piecewise Arrhenius trend (*solid line*) with a crossover at ~15°C. (*C*) Direct comparison of the trends in (*A*) (*dashed gray line*) and (*B*) (*solid black line*) on the logarithmic Arrhenius plot. Inset: ratio of the fit curves obtained in (*A*) and (*B*) plotted on a linear scale. (*D*) Yeast cytoplasmic dynein velocity and fit to a piecewise Arrhenius trend (*solid line*) with a crossover at ~8°C (activation energy 50.5 kJ/mol and 151.5 kJ/mol above and below 8°C, respectively). (*E*) Arrhenius plot of (*D*). Error bars, mean ± SE.

dynein (in the absence of any regulatory cofactors; Fig. S1) were similar between ~15°C and ~27°C (Fig. 1 *A*) and followed a simple Arrhenius temperature dependence in this range. The activation energy extracted from the Arrhenius fit to the velocity data was ~65 kJ/mol, which is slightly higher than that previously reported for another kinesin-1 isoform, KIF5B (9). This trend persisted above 27°C when velocity was measured within ~10 min of temperature change. However, beads were increasingly immotile on MTs afterward, consistent with previous reports of kinesin denaturation at elevated temperatures (8,10). The activation energy for mammalian cytoplasmic dynein above ~15°C was just slightly below that of KIF5A: ~59 kJ/mol and dynein showed no signs of motor degradation up to 37°C.

In contrast to kinesin-1, the velocity of mammalian cytoplasmic dynein (but not kinesin-1) crossed over to a distinct Arrhenius trend below 15°C (Fig. 1, *B* and *C*) with an effective activation energy of ~154 kJ/mol. The net effect was that the dynein velocity declined far more quickly than the kinesin velocity (Fig. 1 *C*). To test whether the rapid decline in velocity at low temperatures is a universal feature of cytoplasmic dyneins, we measured the temperature dependence of velocity for a minimal recombinant *S. cerevisiae* cytoplasmic dynein construct whose movement has biophysical characteristics similar to those of native yeast dynein (15). We found that this dynein also showed a break from simple Arrhenius behavior, but at a much lower temperature: the Arrhenius trend at high temperatures had an activation energy of 50.5 kJ/mol above 8°C and 151.5 kJ/mol below that point (Fig. 1, *D* and *E*).

The striking divergence between dynein and kinesin velocities at low temperatures prompted us to examine whether other key motility parameters showed a comparable change at low temperatures (Fig. 2). We found that cytoplasmic dynein's processivity was 0.69 ± 0.09 μm/s at 10°C. This value is within error bars of the processivity measured for identically purified cytoplasmic dynein at room temperature (0.74 ± 0.08 μm/s (13)). We observed a statistically significant decline in processivity for kinesin-1, from 841.5 ± 0.2 μm/s at room temperature to 497.7 ± 0.09 μm/s at 5°C, confirming a previous qualitative observation of a decline in kinesin's processivity with temperature (10). We also measured kinesin (Fig. 2 *D*) and dynein (Figs. 2 *E* and S2) force production at the lowest temperatures where motility was fast enough to allow for reliable force measurements, and observed no statistically significant changes relative to room temperature. In the case of KIF5A kinesin-1, this parallels and slightly extends a previous report for KIF5B (10).

Among the above results, the divergence of kinesin-1 and cytoplasmic dynein velocities at low temperatures stands out as the major qualitative effect because dynein-based motility essentially shuts down below 15°C. By comparison, the decline of kinesin's processivity is significant, but is not sufficient to effectively abrogate transport. This contrast

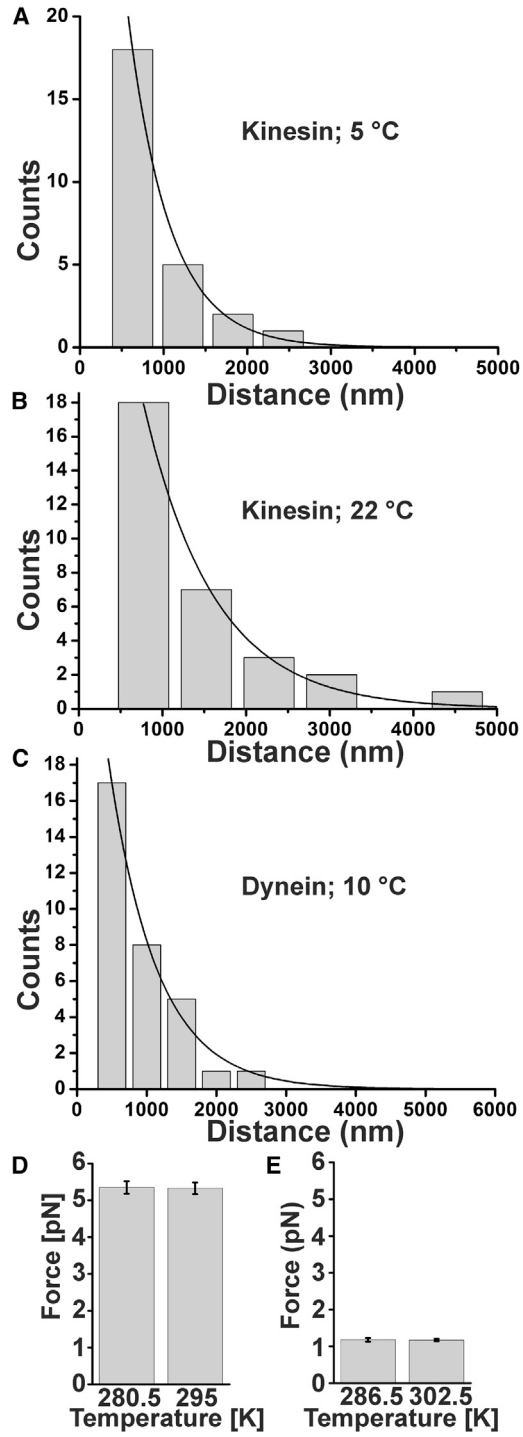

FIGURE 2 Temperature dependence of kinesin and mammalian cytoplasmic dynein processivity and stall force. (*A* and *B*) Kinesin processivity at 5°C (*A*) is 497.7 ± 0.09 μm/s, which is significantly lower than the 841.5 ± 0.2 μm/s obtained at room temperature (*B*). (*C*) Dynein processivity is 0.69 ± 0.09 μm/s at 10°C. Error bars, mean ± SE. (*D* and *E*) Force production by single kinesin (*D*) and mammalian cytoplasmic dynein (*E*) motors (kinesin: 5.3 ± 0.2 pN at 295 K vs. 5.2 ± 0.2 pN at 280.5 K; dynein: 1.2 ± 0.1 pN at 286.5 K vs. 1.2 ± 0.1 pN at 302.5 K; error bars: mean ± SE).

suggests that the net velocities of cargos driven by heterogeneous ensembles of cytoskeletal motors should show an unusual temperature dependence. Without intracellular regulation, kinesin (but not dynein) could effectively move along MTs at low temperatures. Therefore, we expect that cargos that show net retrograde motion at room temperature will move in the anterograde direction at low temperatures. As dynein activity becomes negligible with decreasing temperature, its main contribution to cargo transport will increasingly consist of just binding-unbinding dynamics. In cases where the force production of kinesins and dyneins on the same cargo is balanced (so that four to six dyneins are available for transport versus each kinesin (6,7)), we expect that kinesin activity will almost always be opposed by a team of bound dynein motors, and therefore its role will be to bias the cargo position toward the MT plus end so that rebinding events for dynein motors will be biased in that direction. As a result, this transport has the essential character of a Brownian ratchet whereby the random attachment-detachment kinetics is rectified by an enzymatically active agent.

The effect predicted above is essentially qualitative. Consider motor ensembles in which dynein motors dominate transport at room temperature. If the dyneins shut down at low temperature, then, absent additional regulation, the kinesins would be expected to win by default (using sports terminology). We therefore expect that the prediction would be broadly applicable for biological transport, even though, e.g., dynein's processivity can be modulated substantially by its cofactors (26,27). However, it is also clear that the predicted effect should be amenable to regulation, including regulation of motor parameters other than velocity. For example, kinesin-based cargo motility can effectively shut down at low temperature if, e.g., the motor processivity drops to near zero. We therefore decided to explore quantitatively the range of conditions in which our predicted effect could be observable. To do this, we performed bidirectional transport simulations for a variable number of kinesin and dynein motors under a variety of realistic motor parameters. In this report, we focus primarily on the case of one kinesin versus four dyneins; however, we also considered a case in which kinesin and dynein forces were balanced, and an example of such a simulation is shown in Fig. S3.

Our simulations indeed demonstrate the change in transport directionality at low temperatures (Figs. 3 and 4; see Supporting Materials and Methods for simulation details). Furthermore, they predict this effect not only for realistic motor parameters (Figs. S4 and S5) but also for parameter values that were recently obtained in the presence of dynein cofactors:

Processivity. Our simulations revealed reversals in transport directionality even when dynein processivity was changed by as much as 10-fold (Figs. 4 *B* and S6) (26,27). In addition, we also expect the effect to be present regardless of whether kinesin's processivity is temperature dependent (Fig. S4) or independent (Fig. S5).

Motor force production. Reversals in transport directionality also occurred in simulations in which dynein and kinesin motor stall forces were balanced. The stall force of 2.5 pN was chosen to model the case in Ref. (28) (Fig. S3); however, a different stall force choice would not alter the conclusions qualitatively.

Motor persistence. The detachment rate of kinesin and dynein motors is known to strongly affect the character of bidirectional transport (24). Therefore, we simulated ensemble motor motility using detachment kinetics measured previously by Kunwar et al. (24). The reversal of directional bias with temperature was again a prominent feature of the simulated cargo tracks (Fig. 4, *A–C*). Simulations in which kinesin and dynein persistence under superstall load was varied also showed a directionality reversal with temperature.

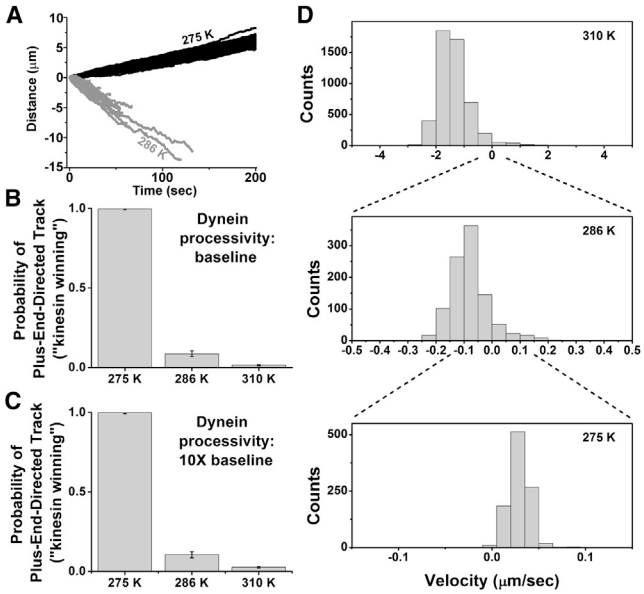

FIGURE 3 Simulations of cargo transported by a team of one kinesin and four dyneins (5 pN and 1.25 pN stall force, respectively). Motors were simulated using the anisotropic force-detachment relationship (Fig. S4 and Supporting Materials and Methods). (*A*) Independent traces of simulated bead motion at 275 K (*black*) and 286 K (*dark gray*) are shown superimposed (100 traces for each temperature). (*B* and *C*) Probability that a simulated trace will have a positive final location (i.e., the probability of kinesin winning) for (*B*) baseline and (*C*) 10× higher dynein processivity values at high, intermediate, and low temperatures (310 K, 286 K, 275 K). (*D*) Transport velocity histograms illustrate that the directional preference reverses sign as a function of temperature. Note that the velocity undergoes large changes with temperature, necessitating the rescaling of the *x* axis.

DISCUSSION

We have observed that mammalian kinesin-1 and cytoplasmic dynein show divergent mechanochemical activity

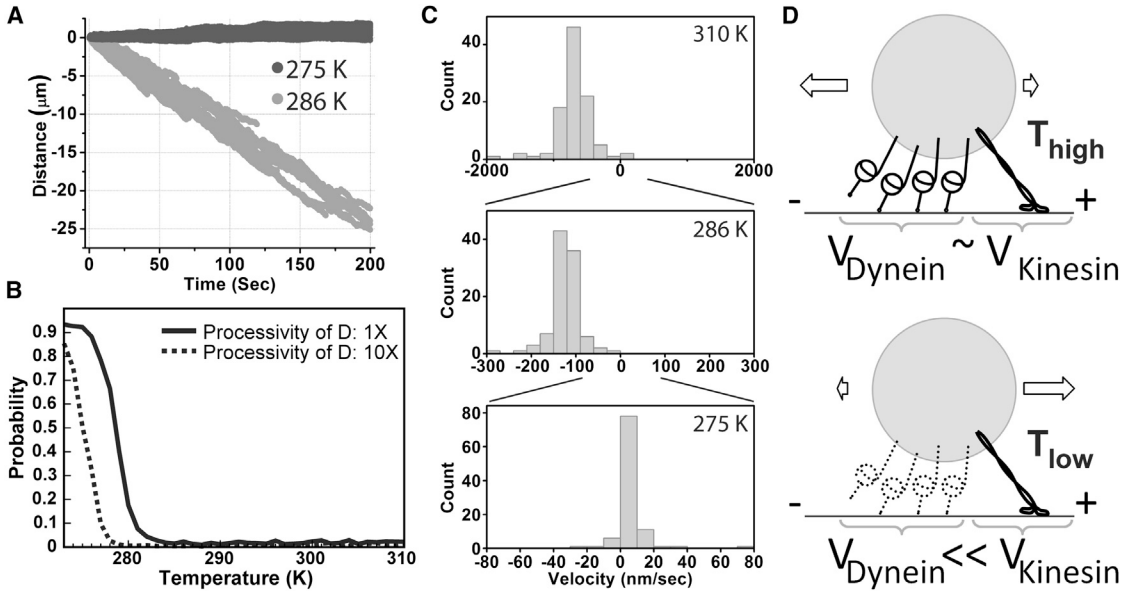

FIGURE 4 Simulations of cargo transported by a team of one kinesin and four dyneins (5 pN and 1.25 pN stall force, respectively). Motors were simulated using the isotropic force-detachment relationship (model B, Fig. S5). (*A*) Independent traces of simulated bead motion at 275 K (*dark gray*) and 286 K (*light gray*) are shown superimposed (100 traces for each temperature). (*B*) Probability that a simulated trace will have a positive final location (i.e., the probability of kinesin winning) for baseline (1×: *solid line*) and 10× (*dashed line*) higher dynein processivity values. (*C*) Transport velocity histograms reveal that the directional preference reverses sign as a function of temperature. Note that the velocity undergoes large changes with temperature, necessitating the rescaling of the *x* axis. (*D*) Model: when all motors are active at high temperatures (*top*), some ensembles of kinesin and dynein motors will exhibit motility with an overall bias in the minus-end direction on MTs. However, at low temperatures (*bottom*), dynein steps dramatically more slowly than kinesin, leading to an overall transport bias in the plus-end direction, as well as other potentially observable effects (Movies S1, S2, and S3).

trends. The extremely high activation energy for dynein at low temperatures means that within just a few degrees below 15°C, dynein transport essentially shuts down relative to kinesin motility. This observation naturally lends itself to understanding the mechanistic origins behind the long-standing mystery of cold block, a phenomenon in which fast axonal transport (FAT) in mammals ceases below ~12°C, even in animals capable of hibernating (2,29). It has long been established that cold block cannot be explained by MT depolymerization at low temperatures (29). On the other hand, the strong temperature-dependent decline of dynein-based motility would likely be sufficient to cause a shutdown of dynein-based and kinesin-based FAT at low temperatures in vivo: a halt of dynein motility by means other than temperature typically results in a gradual stoppage of kinesin-based transport as well, due to intracellular motor regulation (30).

If our hypothesis is correct, one may expect the dynein activation energy to evolve smoothly through 15°C in organisms that are not prone to cold block. Indeed, although we observe a similar piecewise Arrhenius trend in yeast cytoplasmic dynein, the trend break occurs at 8°C. This trend break likely carries no physiological implications: cytoplasmic dynein is nonessential in yeast (31), and in addition, MT stability (and hence MT-associated activity) is compromised at such low temperatures (32).

Many biological enzymes show a simple Arrhenius trend for enzymatic activity near room or physiological temperature but break from this trend at low temperatures, i.e., they have a limited thermal dynamic range (33). We propose that the architecture of cytoplasmic dynein allows for tuning of this dynamic range between species. In principle, the observed cytoplasmic dynein velocity trend break at low temperatures could be due to either a change in the enzymatic rate of the motor or a change in mechanochemical coupling between the two motor domains of dynein. In this context, it is very suggestive that the activation energies above and below the break temperature are extremely close for mammalian and yeast dyneins, and in particular are very high at low temperatures. Thus, we speculate that the thermal dynamic range of cytoplasmic dyneins may be tunable via the same mechanism. If so, we propose that regulation of dynein's thermal dynamic range could occur via its enzymatic domain(s). The AAA ring of dynein certainly has ample complexity (34) to potentially allow for such a mechanism. Coordination between dynein heavy chains is less likely to be the culprit because the velocity of cytoplasmic dyneins is not strongly dependent on the amount of coordination between motor domains (35–37). Furthermore, if such coordination were important under some conditions, one might naively expect the effect to be different for an artificial dimer (the yeast construct we examined) versus a full cytoplasmic dynein complex.

It is also worthwhile to contrast our observations with recent work (36) that identified the C-terminus domain of the dynein heavy chain (present in mammalian but not yeast

motors) as a regulator of dynein's top force production, which likely accounts for the observed differences between yeast and mammalian motor stall forces. It is conceivable that this effect is due to an interaction between the C-terminus domain and the AAA1 domain (36). However, the unchanged activation energy for motor velocity between yeast and mammalian dynein hints that perhaps the force production is not exclusively set within the enzymatically active part of the motor. For instance, the possibility of the C-terminus domain interacting with dynein's linker domain (directly or indirectly) has been put forth before (37), and an allosteric effect is structurally feasible (38). One can therefore envision scenarios in which the C-terminus domain modulates linker docking. This would be conceptually (though not structurally) similar to what is seen in kinesin, where the cover-neck bundle affects the neck-linker affinity for the motor domain during the powerstroke, thereby directly affecting motor force production (39,40).

Our simulations suggest that the reversal of the overall transport direction as a function of temperature is likely to be a very robust effect. This is because the effect arises with very few extremely relaxed starting assumptions. First, bidirectional transport at room temperature needs to be dominated by dynein—a condition that is known to occur for many intracellular cargos. The specific properties of individual dynein motors (processivity, force production, persistence under load, etc.) are not critically important here. All that critically matters is that the dynein ensemble on average wins over the kinesin ensemble at some temperature above the dynein crossover point. The other thing that is needed for directionality reversal is for dynein to effectively cease motility at low temperatures so that the dynamics of the dynein ensemble would be mostly reduced to simple on/off kinetics. We make explicit assumptions in our simulations about the temperature dependence of the on/off rates of dynein as a function of temperature. However, all we really need is for these rates to not differ by many orders of magnitude from the rates at high temperatures. This is a reasonable assumption in light of our experimental data, and would be expected a priori from general biochemistry considerations. Finally, we need the kinesin ensemble to still be active at low temperatures. With these conditions in place, the net cargo motility at low temperatures arises from random binding and unbinding of dynein motors. Indeed, the average number of engaged dyneins remains nearly identical at low temperatures, but the difference grows appreciably at high temperatures as dynein's processivity increases 10-fold (Fig. S7). This remains true regardless of the force-dissociation model we use for kinesin and dynein motors. The fluctuations are minimally biased by any remnant dynein motility, but they are appreciably biased by the kinesin activity. Our simulations show that regardless of the force-dissociation model we use for kinesin and dynein motors, and for both $1\times$ and $10\times$ choices of dynein processivity, the fraction of time in which kinesin is pulling the cargo with a force equal to or exceeding its stall force grows very gradually as the temperature declines and is above 60% at the lowest temperatures (Fig. S8). Any unbinding dynein motor will diffuse around its anchor point on the cargo, which is displaced however slightly by kinesin motor(s) toward the MT plus end. This dynein is then likely to rebind with an average displacement toward the MT plus end (relative to its previous bound position).

From a biophysics perspective, kinesin activity drives the system far from equilibrium and rectifies the on/off fluctuations of the dynein ensemble. In other words, the multiple motor ensemble at low temperatures behaves mostly as a Brownian ratchet (41), whereas the displacement at high temperatures has a significant or even dominant contribution from the powerstroke mechanism. This transition is at the core of why the effect we propose is robust and likely to be quite insensitive to individual motor properties. What is particularly remarkable about this system is that the transition can happen over a very small temperature window relative to the absolute temperature scale.

Keeping in mind that the directionality reversal is likely to be a robust effect, we propose that temperature regulation may present an opportunity to develop a new approach for probing intracellular transport. The qualitative directionality reversal effect should be observable in cell culture or even in vivo after an acute cold shock to $\leq 10^{\circ}$C. The shock would need to occur much faster than any possible cold-shock protein expression (42) to provide a temporal window during which a plus- versus minus-end-directed motility imbalance would be observable and quantifiable. In addition, cold shock can induce cell permeabilization with resultant changes in, e.g., metal ion concentrations and cellular pH (42)—all factors that need to be controlled for. Despite such immediate experimental challenges, we envision that the above approach will become increasingly feasible when the response of cell culture to cold shock is generally better understood.

Also of note, activation energies are not identical (12) across the many kinesin families. Therefore, even though the velocities of cytoplasmic dynein and KIF5A measured here (Fig. 1) are fairly well matched above 15°C, this situation cannot hold for all kinesins. We thus speculate that in other systems (e.g., motor ensembles including kinesin-3), bidirectional transport likely requires additional regulation to maintain even qualitative homeostasis across the mammalian survival range. Of course, such temperature-based feedback could be used in cells to sense temperature.

The temperature dependence of fast MT-based transport can be far more complex in lower species than in mammals (2). This suggests one of two possibilities. First, it is possible that cytoplasmic dynein, like its axonemal counterpart (43), is thermally adaptable to match the thermal range of its species. A tantalizing alternative is that an

as yet unidentified cofactor(s) can regulate the temperature dependence of dynein motility. This is hinted at by the observation that cold acclimation in poikilotherms can lead to increased rates of FAT at low temperatures (44). Either way, the thermal properties of motor-driven transport and its regulation clearly warrant further study.

SUPPORTING MATERIAL

Supporting Materials and Methods, eight figures, and three movies are available at http://www.biophysj.org/biophysj/supplemental/S0006-3495(16)30664-6.

AUTHOR CONTRIBUTIONS

M.V. initiated and guided the project. W.H. and O.O. performed experiments. A.K. directed and guided the theoretical modeling. A.T. implemented the theoretical modeling and contributed to conceptual model refinement. All authors co-wrote the manuscript.

ACKNOWLEDGMENTS

We thank the members of Dr. Richard Vallee's lab for purifying and supplying the mammalian cytoplasmic dynein motors, Dr. R. McKenney and Dr. R. Vale for the generous gift of purified yeast dynein, and Dr. S. Gross and J. Bergman for helpful discussions.

A.K. is supported in part by the Industrial Research and Consultancy Centre at IIT Bombay and by an Innovative Young Biotechnologist Award from the Department of Biotechnology (grant number BT/06/IYBA/2012). This work was supported by National Science Foundation grant number ENG-1563280 to M.V.

REFERENCES

1. Carey, H. V., M. T. Andrews, and S. L. Martin. 2003. Mammalian hibernation: cellular and molecular responses to depressed metabolism and low temperature. *Physiol. Rev.* 83:1153–1181.
2. Cancalon, P. 1985. Influence of temperature on various mechanisms associated with neuronal growth and nerve regeneration. *Prog. Neurobiol.* 25:27–92.
3. Mallik, R., A. K. Rai, …, A. Kunwar. 2013. Teamwork in microtubule motors. *Trends Cell Biol.* 23:575–582.
4. Gross, S. P., M. Vershinin, and G. T. Shubeita. 2007. Cargo transport: two motors are sometimes better than one. *Curr. Biol.* 17:R478–R486.
5. Müller, M. J. I., S. Klumpp, and R. Lipowsky. 2010. Bidirectional transport by molecular motors: enhanced processivity and response to external forces. *Biophys. J.* 98:2610–2618.
6. Soppina, V., A. K. Rai, …, R. Mallik. 2009. Tug-of-war between dissimilar teams of microtubule motors regulates transport and fission of endosomes. *Proc. Natl. Acad. Sci. USA.* 106:19381–19386.
7. Hendricks, A. G., E. Perlson, …, E. L. F. Holzbaur. 2010. Motor coordination via a tug-of-war mechanism drives bidirectional vesicle transport. *Curr. Biol.* 20:697–702.
8. Böhm, K. J., R. Stracke, …, E. Unger. 2000. Effect of temperature on kinesin-driven microtubule gliding and kinesin ATPase activity. *FEBS Lett.* 466:59–62.
9. Kawaguchi, K., and S. Ishiwata. 2000. Temperature dependence of force, velocity, and processivity of single kinesin molecules. *Biochem. Biophys. Res. Commun.* 272:895–899.
10. Kawaguchi, K., and S. Ishiwata. 2001. Thermal activation of single kinesin molecules with temperature pulse microscopy. *Cell Motil. Cytoskeleton.* 49:41–47.
11. Zhao, Y. C., F. J. Kull, and J. C. Cochran. 2010. Modulation of the kinesin ATPase cycle by neck linker docking and microtubule binding. *J. Biol. Chem.* 285:25213–25220.
12. Adio, S., and G. Woehlke. 2009. Properties of the kinesin-3 NcKin3 motor domain and implications for neck function. *FEBS J.* 276:3641–3655.
13. McKenney, R. J., M. Vershinin, …, S. P. Gross. 2010. LIS1 and NudE induce a persistent dynein force-producing state. *Cell.* 141:304–314.
14. Smith, T. E., W. Hong, …, M. Vershinin. 2013. Single-molecule inhibition of human kinesin by adociasulfate-13 and -14 from the sponge Cladocroce aculeata. *Proc. Natl. Acad. Sci. USA.* 110:18880–18885.
15. Reck-Peterson, S. L., A. Yildiz, …, R. D. Vale. 2006. Single-molecule analysis of dynein processivity and stepping behavior. *Cell.* 126:335–348.
16. Vershinin, M., B. C. Carter, …, S. P. Gross. 2007. Multiple-motor based transport and its regulation by Tau. *Proc. Natl. Acad. Sci. USA.* 104:87–92.
17. Svoboda, K., C. F. Schmidt, …, S. M. Block. 1992. Conformation and elasticity of the isolated red blood cell membrane skeleton. *Biophys. J.* 63:784–793.
18. Mao, H., J. R. Arias-Gonzalez, …, C. Bustamante. 2005. Temperature control methods in a laser tweezers system. *Biophys. J.* 89:1308–1316.
19. Bennet, M. A., P. R. Richardson, …, A. C. Jones. 2011. Optically trapped microsensors for microfluidic temperature measurement by fluorescence lifetime imaging microscopy. *Lab Chip.* 11:3821–3828.
20. Fernandez, A. C., and G. D. J. Phillies. 1983. Temperature dependence of the diffusion coefficient of polystyrene latex spheres. *Biopolymers.* 22:593–595.
21. Müller, C. B., and W. Richtering. 2008. Sealed and temperature-controlled sample cell for inverted and confocal microscopes and fluorescence correlation spectroscopy. *Colloid Polym. Sci.* 286:1215–1222.
22. Chung, K., J. K. Cho, …, H. Lu. 2009. Three-dimensional in situ temperature measurement in microsystems using Brownian motion of nanoparticles. *Anal. Chem.* 81:991–999.
23. Li, S., K. Zhang, …, H. Yang. 2007. Single quantum dots as local temperature markers. *Nano Lett.* 7:3102–3105.
24. Kunwar, A., S. K. Tripathy, …, S. P. Gross. 2011. Mechanical stochastic tug-of-war models cannot explain bidirectional lipid-droplet transport. *Proc. Natl. Acad. Sci. USA.* 108:18960–18965.
25. Kunwar, A., M. Vershinin, …, S. P. Gross. 2008. Stepping, strain gating, and an unexpected force-velocity curve for multiple-motor-based transport. *Curr. Biol.* 18:1173–1183.
26. Schlager, M. A., H. T. Hoang, …, A. P. Carter. 2014. In vitro reconstitution of a highly processive recombinant human dynein complex. *EMBO J.* 33:1855–1868.
27. McKenney, R. J., W. Huynh, …, R. D. Vale. 2014. Activation of cytoplasmic dynein motility by dynactin-cargo adapter complexes. *Science.* 345:337–341.
28. Shubeita, G. T., S. L. Tran, …, S. P. Gross. 2008. Consequences of motor copy number on the intracellular transport of kinesin-1-driven lipid droplets. *Cell.* 135:1098–1107.
29. Brimijoin, S., J. Olsen, and R. Rosenson. 1979. Comparison of the temperature-dependence of rapid axonal transport and microtubules in nerves of the rabbit and bullfrog. *J. Physiol.* 287:303–314.
30. Yi, J. Y., K. M. Ori-McKenney, …, R. B. Vallee. 2011. High-resolution imaging reveals indirect coordination of opposite motors and a role for LIS1 in high-load axonal transport. *J. Cell Biol.* 195:193–201.
31. Eshel, D., L. A. Urrestarazu, …, I. R. Gibbons. 1993. Cytoplasmic dynein is required for normal nuclear segregation in yeast. *Proc. Natl. Acad. Sci. USA.* 90:11172–11176.

32. Bellocq, C., I. Andrey-Tornare, …, S. J. Edelstein. 1992. Purification of assembly-competent tubulin from Saccharomyces cerevisiae. *Eur. J. Biochem.* 210:343–349.

33. Fink, A. L., and S. J. Cartwright. 1981. Cryoenzymology. *CRC Crit. Rev. Biochem.* 11:145–207.

34. Qiu, W., N. D. Derr, …, S. L. Reck-Peterson. 2012. Dynein achieves processive motion using both stochastic and coordinated stepping. *Nat. Struct. Mol. Biol.* 19:193–200.

35. DeWitt, M. A., A. Y. Chang, …, A. Yildiz. 2012. Cytoplasmic dynein moves through uncoordinated stepping of the AAA+ ring domains. *Science.* 335:221–225.

36. Nicholas, M. P., P. Höök, …, A. Gennerich. 2015. Control of cytoplasmic dynein force production and processivity by its C-terminal domain. *Nat. Commun.* 6:6206.

37. Höök, P., A. Mikami, …, R. B. Vallee. 2005. Long range allosteric control of cytoplasmic dynein ATPase activity by the stalk and C-terminal domains. *J. Biol. Chem.* 280:33045–33054.

38. Kon, T., T. Oyama, …, G. Kurisu. 2012. The 2.8 Å crystal structure of the dynein motor domain. *Nature.* 484:345–350.

39. Hwang, W., M. J. Lang, and M. Karplus. 2008. Force generation in kinesin hinges on cover-neck bundle formation. *Structure.* 16:62–71.

40. Khalil, A. S., D. C. Appleyard, …, M. J. Lang. 2008. Kinesin's cover-neck bundle folds forward to generate force. *Proc. Natl. Acad. Sci. USA.* 105:19247–19252.

41. Cubero, D., and F. Renzoni. 2016. Brownian Ratchets: From Statistical Physics to Bio and Nano-motors, 1st ed. Cambridge University Press, Cambridge, UK.

42. Underhill, M. F., and C. M. Smales. 2007. The cold-shock response in mammalian cells: investigating the HeLa cell cold-shock proteome. *Cytotechnology.* 53:47–53.

43. King, S. M., S. P. Marchese-Ragona, …, H. W. Detrich, 3rd. 1997. Inner and outer arm axonemal dyneins from the Antarctic rockcod Notothenia coriiceps. *Biochemistry.* 36:1306–1314.

44. Edström, A., and M. Hanson. 1973. Temperature effects on fast axonal transport of proteins in vitro in frog sciatic nerves. *Brain Res.* 58:345–354.

Biophysical Journal, Volume *111*

Supplemental Information

The Effect of Temperature on Microtubule-Based Transport by Cytoplasmic Dynein and Kinesin-1 Motors

Weili Hong, Anjneya Takshak, Olaolu Osunbayo, Ambarish Kunwar, and Michael Vershinin

Supporting Material

Title:

The effect of temperature on microtubule-based molecular motor transport

Authors

W. Hong, A. Takshak, O. Osunbayo, A. Kunwar, M. Vershinin

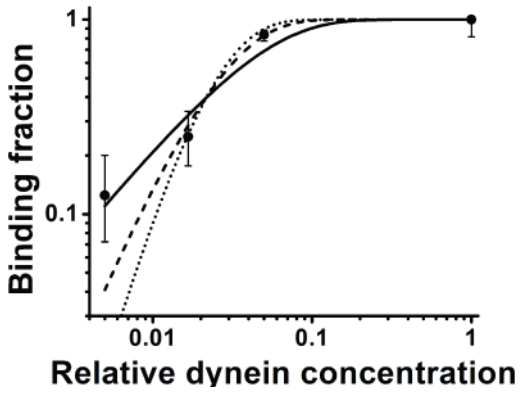

Fig. S1 Single motor activity of cytoplasmic dynein. The binding fraction data for dynein is best fit by single molecule Poisson distribution 1-exp(-n/b) but not by two molecule distribution: 1-exp(-n/b)-(n/b)exp(-n/b) or three molecule distribution 1-exp(-n/b)-(n/b)exp(-n/b))-(n/b)2exp(-n/b)/2 (solid, long dash and short dash curves respectively). Error bars: CI for binomial distribution.

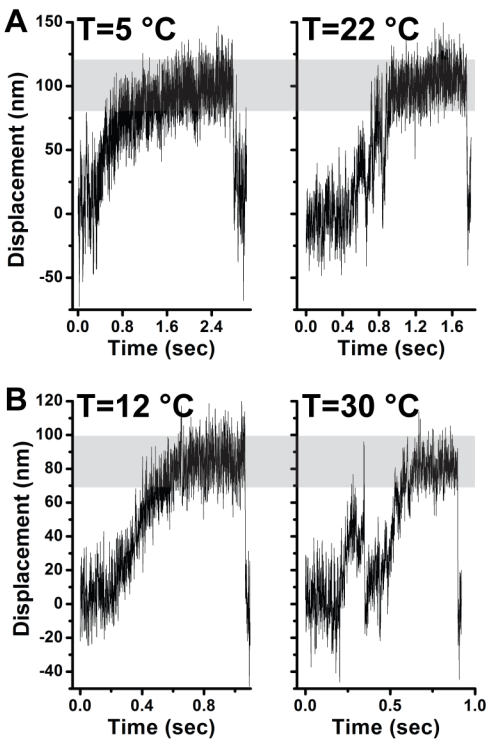

Figure S2. Single motor stalls were experimentally observed for both dynein and kinesin. The stalls were quantified (Fig. 2) for temperatures where motility allowed efficient data collection. Representative examples of motor stall shapes are reported here. Representative stall events for kinesin (A) and dynein (B) motors are shown.

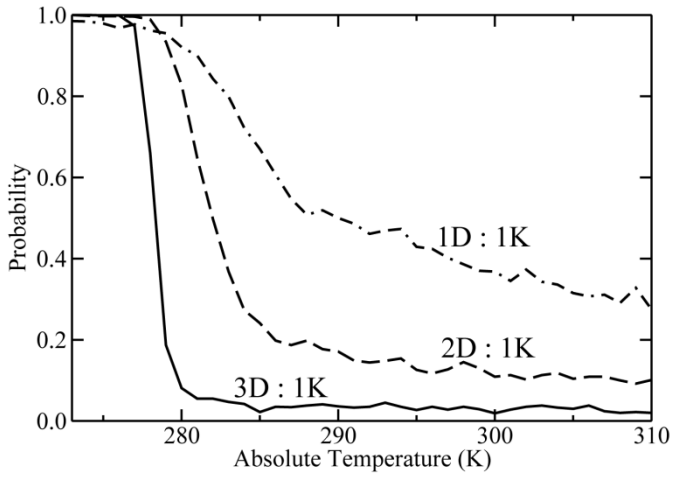

Figure S3. Kinesin “winning probability” for different motor ensembles as a function of temperature. Here, individual dynein (D) and kinesin (K) motor forces were assumed balanced at 2.5 pN. The number of motors in an ensemble is as indicated for each curve. Simulations were performed using the *in-vivo* kinesin-1 and *in-vivo* cytoplasmic dynein parameters given in Text S1 in the Supplementary Material.

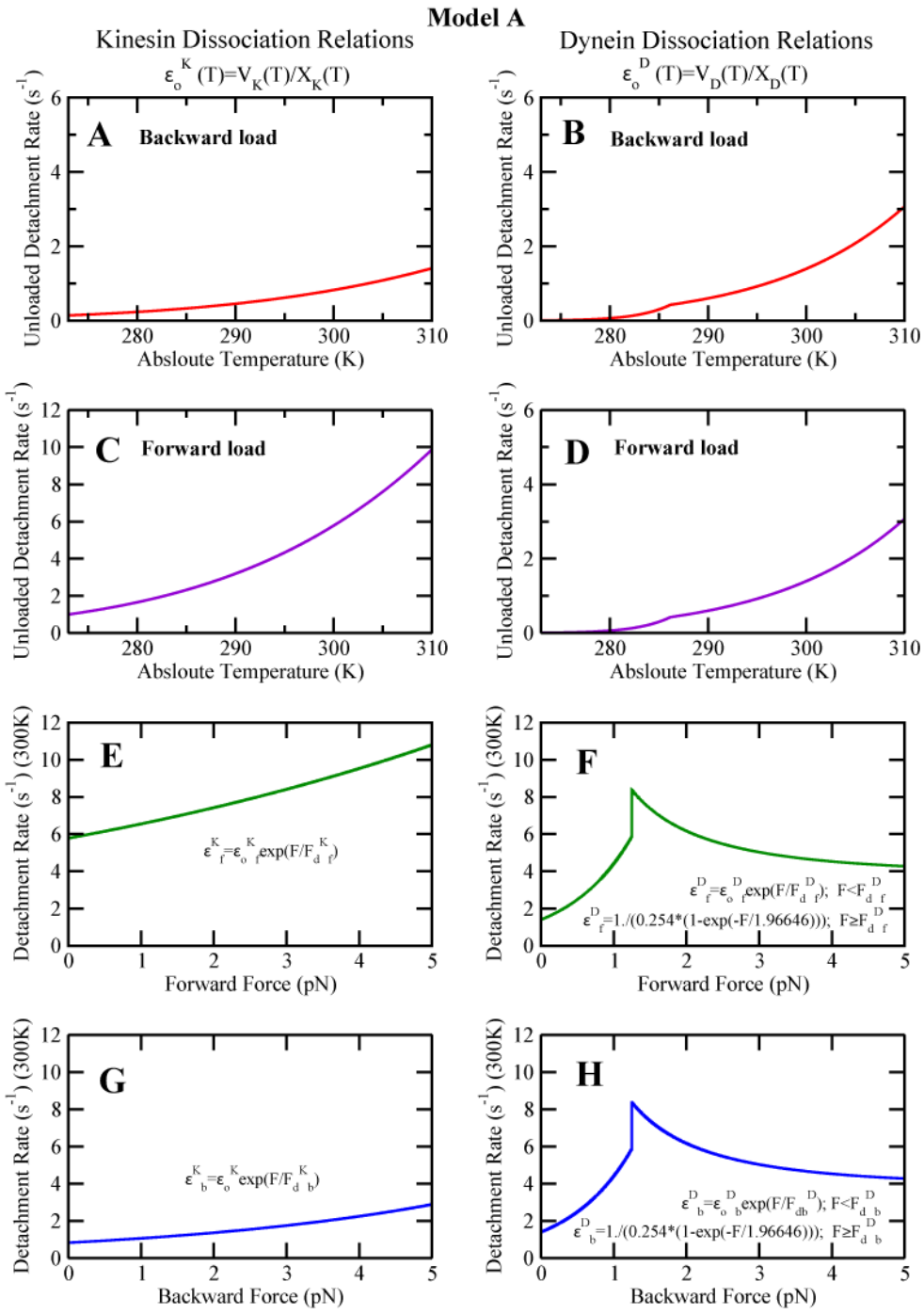

Figure S4. Force- dissociation relations for kinesin-1 and cytoplasmic dynein used in this work for simulations in Fig.3 and the figures in the supplement.

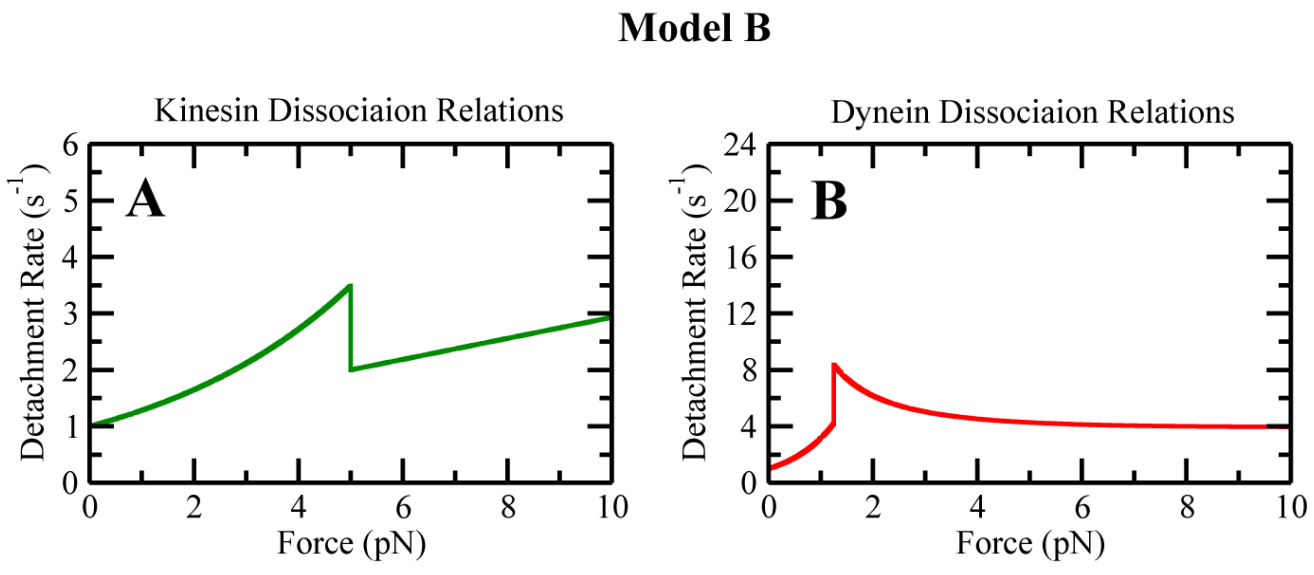

Figure S5: Simulations results in Fig. 4 were performed using detachment kinetics shown in (A) and (B) for Kinesin and Dynein motors respectively.

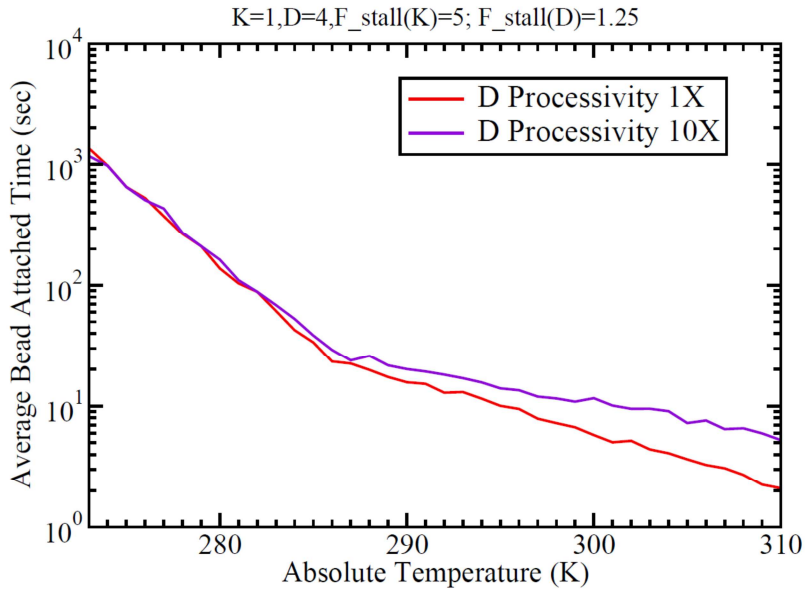

Figure S6. Cargo attachment times show signature of dynein velocity crossover for ensembles of 4 dyneins (1.25 pN stall) and 1 kinesin (5 pN stall) (compare with Fig. 3B). 10X means dynein processivity was increased by a factor of 10.

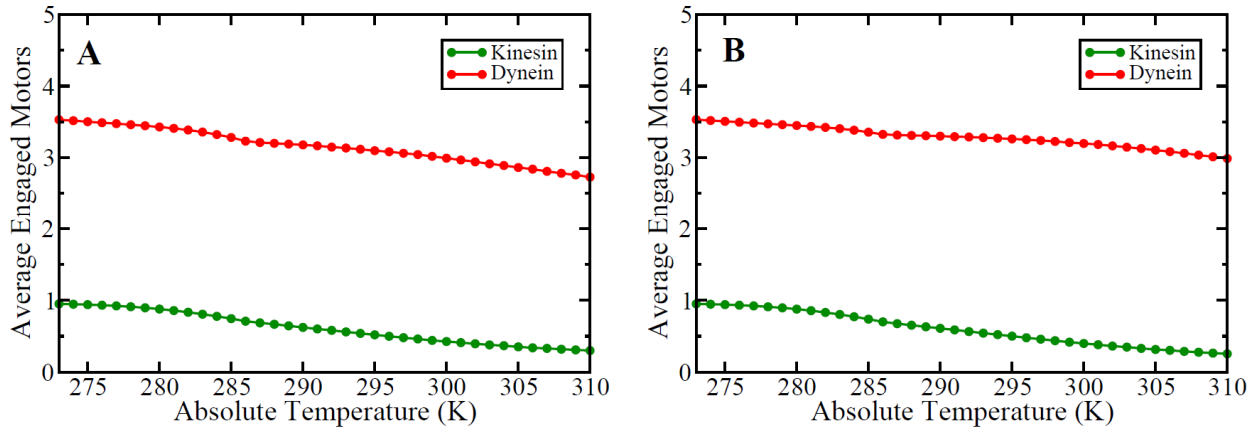

Figure S7. Average ensemble composition for engaged motors. The average number of engaged kinesin and dyneins was calculated for a cargo carrying 4 kinesins and 1 dynein using Model A parameters. We have used 1X (A) and 10X (B) dynein processivity in the simulations but only minor changes at higher temperatures are apparent in the simulated ensembles.

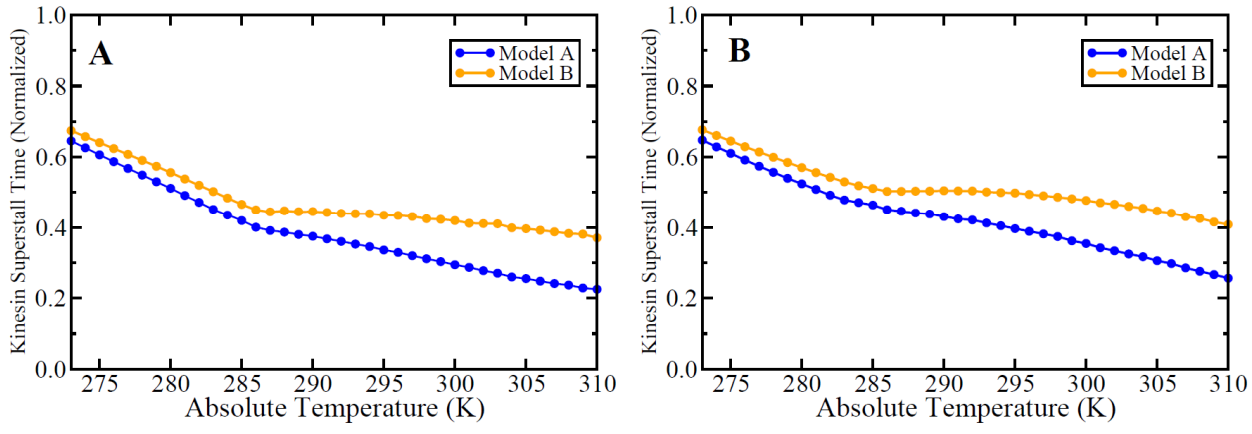

Figure S8. The fraction of time kinesin spends in superstall regime. The gradual decrease in kinesin superstall time fraction as temperature increases is similar for simulations with 1X (A) and 10X (B) dynein processivity.

Movie S1. Simulations of bi-directional transport (Fig. 3) driven by 4 dynein motors and one kinesin at 273 K yielded simulated positions of all motors and the cargo. This data for one representative simulation is shown in movie form (dynein – red, kinesin – green, cargo – black). Motors which are not attached to the MT are not shown so that the number of motors visualized may change from frame to frame.

Movie S2. Simulations of bi-directional transport (Fig. 3) driven by 4 dynein motors and one kinesin at 286 K yielded simulated positions of all motors and the cargo. This data for one representative simulation is shown in movie form (dynein – red, kinesin – green, cargo – black). Motors which are not attached to the MT are not shown so that the number of motors visualized may change from frame to frame.

Movie S3. Simulations of bi-directional transport (Fig. 3) driven by 4 dynein motors and one kinesin at 310 K yielded simulated positions of all motors and the cargo. This data for one representative simulation is shown in movie form (dynein – red, kinesin – green, cargo – black). Motors which are not attached to the MT are not shown so that the number of motors visualized may change from frame to frame.

Text S1.

- **Monte-Carlo Simulation of Temperature Dependent Bi-directional Cargo Motility**

To simulate bidirectional cargo under *in-vitro* and *in-vivo* conditions, we considered a cargo having Kinesin and Dynein motors with various parameters (listed in appropriately labeled Tables later). A Cargo with 'n' Kinesin (Kinesin-1) and 'm' Dynein Motors (Cytoplasmic Dynein) instantaneously attached to the microtubule is abbreviated as (K=n, D=m) in the main text. We used the stochastic model developed by Kunwar *et al.* in [1,2] to simulate the temperature dependence of bidirectional cargo transport by multiple molecular motors of opposing types. The model uses experimentally established parameters for motor function and accurately accounts for many prior experimental results, e.g. the force-velocity curve for kinesin-1[3]. We developed two distinct models to simulate bidirectional cargo motility depending on the detachment kinetics of the involved motors.
In Model A, we considered the anisotropic detachment of Kinesin motors under forward and backward loads measured by Andreasson *et al.* [4], and temperature dependence of unloaded detachment rate of both Kinesin and Dynein motors. While in Model B, we considered isotropic detachment for both sets of motors and used earlier measured detachment kinetics of Kinesin and Dynein motors by Kunwar *et al.* [1].

The common features of both Model A and Model B are briefly described below:

For both models, simulations were performed for temperatures (T) in the range of 273K-310K (0ºC-37ºC) in intervals of 1K. A maximum N number of Kinesin motors and M number of Dynein motors were put on cargo. The motors of both types were modeled as special linkages which exert a restoring force only when they are stretched beyond their rest length and buckle without any resistance when compressed [1,2].The spring constants for both motor types was taken to be k=0.32pN/nm [1,2].The radius of the cargo (r) was taken to be 0.25 µm and the medium viscosity η to be 0.003Pa-s. In our simulations, the velocity of Kinesin and Dynein was dependent on both load felt by the motor, and system temperature.

For both models, Kinesin was considered a simple Arrhenius enzyme whose maximum velocity at zero load (V_o^K) varied with absolute temperature as:

$$V_o^K(T) = A^K * \exp(-E_a^K/(k_B T))$$

Where A^K is the Arrhenius constant for Kinesin; E_a^K is its Activation energy; k_B is Boltzmann Constant and T is the Absolute Temperature. However, Dynein was considered a complex Arrhenius Enzyme because the temperature dependence of its velocity has two distinct domains with two Activation energies: below a critical temperature T_c, Dynein velocity at zero load (V_o^D) is given by

$$V_o^D(T) = A^D * \exp(-E_a^{D1}/(k_B T))$$

While above T_c,

$$V_o^D(T) = A^D * \exp((E_a^{D2} - E_a^{D1})/T_o) * \exp(-E_a^{D2}/(k_B T))$$

Where A^D is the Arrhenius constant for Dynein and E_a^{D1} and E_a^{D2} are its two Activation energies. Kinesin's velocity was considered to reduce sub-linearly with load/ force (F) as

$$V^K(F,T) = V_o^K(T) * (1 - (F/F_s^K)^2)$$

While for dynein, the force-velocity relation was super-linear:

$$V^D(F,T) = V_o^D(T) * (1 - (F/F_s^D)^{0.25})$$

In both models, each simulation was started with all motors attached to the microtubule. Attached Kinesin and Dynein motors start to step along microtubule in opposite directions with stepping rates obtained from force velocity relations i.e. dividing velocity at any given force and temperature by motor step size. Thus motor can get engaged in a tug-of-war if both sets of motors are simultaneously attached to the microtubule. While engaged in a tug-of-war, a motor could experience load in the same or opposite direction of its stepping. It was assumed that forward load had no effect on the motor velocity and only backward load reduced its velocity/stepping rate.

In our models, individual attached motors can either step on the microtubule or detach from the microtubule, at each time step. Conversely, at each time step unattached motors can reattach to the microtubule with re-attachment probabilities determined from their respective on-rates. The cargo continues along the microtubule, instantaneously driven by a number n of engaged Kinesin motors and/or m number of Dynein motors (where $n \leq N$, $m \leq M$ respectively), and is updated at every time step according to motors'

attachment and detachment events, until the simulation ends, or n+m= 0; indicating all motors have fallen off the microtubule.

In our simulations, motor's detachment rate was influenced by both forward as well as backward load. The detachment kinetics of individual type of motors was different in the two models.

In Model A, the unloaded detachment rate of both sets of motors was considered temperature dependent; and was explicitly calculated by dividing the velocity of motors at a particular temperature T by the travel distance (runlength) at that T:

$$\epsilon_o^K(T) = V_o^K(T) / X_o^K(T) \quad (1)$$

Where $V_o^K(T)$ and $X_o^K(T)$ are the unloaded velocity and runlength of Kinesin at a particular temperature T. $X_o^K(T)$ was assumed to be varying exponentially with temperature as:

$$X_o^K(T) = 0.1*\exp(T/32.64)$$

Further, the detachment kinetics of Kinesin was taken to be anisotropic as studied by Andreasson *et al.* [4]. Anisotropic means that the detachment kinetics was different under the influence of forward and backward loads experienced by the motor. A forward load is the one which the motor feels in the same direction as its stepping; while the backward load opposes/hinders motor's stepping. For Kinesin, the detachment kinetics was uniformly exponential throughout for both forward and backward loads [4]. The forward ($F_d^K{}_f$) and backward detachment forces ($F_d^K{}_b$) for Kinesin were considered to be constant (temperature independent) at 8pN [4] and 4pN [1] respectively. Thus the expressions for Kinesin detachment (as a function of both force and temperature) are:

$$\epsilon^K{}_f(F,T)=\epsilon_o^K{}_f(T)*\exp(F/F_d^K{}_f) \quad \text{forward loads (2)}$$

$$\epsilon^K{}_b(F,T)=\epsilon_o^K{}_b(T)*\exp(F/F_d^K{}_b) \quad \text{backward loads (3)}$$

Similarly, the temperature dependence of unloaded detachment rate of Dynein was modeled as:

$$\epsilon_o^D(T) = V_o^D(T) / X_o^D(T) \quad (4)$$

Where the value of $X_o^D(T)$ was taken to be constant at 689 nm. The detachment kinetics of Dynein was considered isotropic as in [1,2], i.e., the detachment kinetics was similar for both forward and backward loads. Also, the detachment kinetics was different for sub-stall and super-stall regimes for both types of loads. The rate of detachment of Dynein motors was taken to be increasing exponentially with load up to stall force (i.e.

$F<F_s^D$ for both forward and backward loads. For loads greater than or equal to single motor stall force experimentally-measured detachment rates were used [1]. The forward ($F_d^D{}_f$) and backward detachment forces ($F_d^D{}_b$) for Dynein were considered to be constant (temperature independent) as for Kinesin; however, their magnitudes were the same at 0.87pN [1,2]. Thus the expressions for Dynein detachment (as a function of both force and temperature) are:

$$\epsilon^D{}_f(F,T)=\epsilon_o{}^D{}_f(T)*\exp(F/F_d^D{}_f) \quad \text{sub-stall forward loads (5)}$$

$$\epsilon^D{}_f(F,T)=1./(0.254*(1.-\exp(-F/1.96646))) \quad \text{super-stall forward loads (6)}$$

$$\epsilon^D{}_b(F,T)=\epsilon_o{}^D{}_b(T)*\exp(F/F_d^D{}_b) \quad \text{sub-stall backward loads (7)}$$

$$\epsilon^D{}_b(F,T)=1./(0.254*(1.-\exp(-F/1.96646))) \quad \text{super-stall backward loads (8)}$$

Plots of equations (1)-(8) are shown in Figure S4. Results obtained from simulation of Model A are shown in Fig 3.

In Model B, the rate of detachment of both Kinesin and Dynein motors was taken to be increasing exponentially with load up to stall force (i.e. $F<F_s^K$ for Kinesin and $F<F_s^D$ for Dynein). Thus, the dependence of Kinesin's and Dynein's detachment rate on force up to stall force is given by

$$\epsilon^K=\epsilon_o{}^K\exp(F/F_d^K) \quad (9)$$

$$\epsilon^D=\epsilon_o{}^D\exp(F/F_d^D) \quad (10)$$

For loads greater than or equal to single motor stall force experimentally-measured detachment rates were used [1]. For Kinesin detachment rate in super-stall regime ($F\geq Fs$) is given by

$$\epsilon^K=1.07+0.186*F \quad (11)$$

for *in-vitro* conditions [1]. Experimentally measured detachment rate of Dynein in super-stall regime [1] is given by

$$\epsilon^D=1./(0.254*(1.-\exp(-F/1.96646))) \quad (12)$$

While the rate of detachment of engaged motor was considered to be dependent on load only, there-attachment/on-rates were taken to be independent of both load and Temperature.

Plots of equations (9)-(12) are shown in Figure S5. Results obtained from simulation of Model B are shown in Fig 4.

Time in each simulation was incremented in discrete time intervals of $\Delta t=10^{-5}$s (time step); since this is appropriately smaller than the rate of the fastest event in our system (viz., the detachment rate of Dynein motor at 310K at $F=F_s^D$). The instantaneous probabilities for motor stepping, detachment and reattachment were calculated by multiplying the respective rates with Δt.

Our simulations included the effect of both thermal noise and the viscous drag. The thermal diffusion of the cargo due to T was assumed to be normally distributed with a mean of $(2D\Delta t)$; where D is the temperature-dependent diffusion coefficient of the cargo [1]. D can be calculated via Einstein's Diffusion relation

$$D = (k_B T)/\gamma$$

Where γ is the drag coefficient of the cargo; which for a spherical cargo is a function of the surrounding medium viscosity (η) and the cargo radius (r) as

$$\gamma=6\pi\eta r$$

At each time step Δt, the net force on the cargo due to all attached motors (say F_{net}) was calculated by the algebraic addition of individual forces exerted by all motors. At each time step Δt, net displacement of the cargo due to motors forces and thermal was obtained by adding displacement X_{drift} caused by F_{net} i.e.

$$X_{drift} = (F_{net}/\gamma)*\Delta t$$

and thermal noise X_{random}; which was drawn from a normal distribution with mean square displacement $(2D\Delta t)$.

The final cargo position (x_f) was obtained after the end of simulation and compared with initial position (x_i). If (x_f-x_i) was positive, then Kinesin was considered to win the Tug-of-War; else Dynein. The above procedure was repeated for 1,000 configurations for each Absolute Temperature from 273K-310K; and the probabilities of motor winning as functions of T were analyzed.

- **Parameters used in Simulations for Model A**

1. *In-vitro* Kinesin-1 Parameters

Parameter	**Symbol**	**Magnitude**
Arrhenius Constant	A^K	1.72448E14 nms^{-1}
Activation Energy	E_a^K	65.05869 kJ/mol
Spring Constant	k_K	0.32 pN/nm
Rest Stalk Length	L_K	110 nm
Step size	d_K	8 nm
Stall Force	F_s^K	5.00 pN
Forward Detachment Force	$F_d{}^K{}_f$	8.00 pN
Backward Detachment Force	$F_d{}^K{}_b$	4.00 pN
Rate of attachment	π^K	5 s^{-1}

2. *In-vitro* Cytoplasmic Dynein Parameters

Parameter	**Symbol**	**Magnitude**
Arrhenius Constant	A^D	1.68497E39 nms^{-1}
Critical Temperature	T_C^D	286.1722 K
Activation Energy for $T<T_C^D$	E_a^{D1}	201.3638 kJ/mol
Activation Energy for $T\geq T_C^D$	E_a^{D2}	60.9441 kJ/mol
Spring Constant	k_D	0.32 pN/nm
Rest Stalk Length	L_D	50 nm
Step size	d_D	8 nm
Stall Force	F_s^D	1.25 pN
Forward Detachment Force	$F_d{}^D{}_f$	0.87 pN
Backward Detachment Force	$F_d{}^D{}_b$	0.87 pN
Rate of attachment	π^D	5 s^{-1}
Unloaded Runlength	X_o^D	689 nm

3. *In-vivo* Kinesin-1 Parameters

Parameter	**Symbol**	**Magnitude**
Arrhenius Constant	A^K	1.72448E14 nms^{-1}
Activation Energy	E_a^K	65.05869 kJ/mol
Spring Constant	k^K	0.32 pN/nm
Rest Stalk Length	L_K	110 nm
Step size	d_K	8 nm
Stall Force	F_s^K	2.50 pN
Forward Detachment Force	$F_d{}^K{}_f$	8.00 pN
Backward Detachment Force	$F_d{}^K{}_b$	2.00 pN
Rate of attachment	π^K	5 s^{-1}

4. *In-vivo* Cytoplasmic Dynein Parameters

Parameter	**Symbol**	**Magnitude**
Arrhenius Constant	A^{D}	1.68497E39 nms^{-1}
Critical Temperature	To	286.1722 K
Activation Energy for T<To	E_a^{D1}	201.3638 kJ/mol
Activation Energy for T≥To	E_a^{D2}	60.9441 kJ/mol
Spring Constant	k_D	0.32 pN/nm
Rest Stalk Length	L_D	50 nm
Step size	d_D	8 nm
Stall Force	F_s^{D}	2.50 pN
Forward Detachment Force	$F_d^{D}{}_f$	1.74 pN
Backward Detachment Force	$F_d^{D}{}_b$	1.74 pN
Rate of attachment	π^{D}	5 s^{-1}
Unloaded Runlength	X_o^{D}	689 nm

- **Parameters used in Simulations for Model B**

1. *In-vitro* Kinesin-1 Parameters

Parameter	**Symbol**	**Magnitude**
Arrhenius Constant	A^K	1.72448E14 nms^{-1}
Activation Energy	E_a^K	65.05869 kJ/mol
Spring Constant	k_K	0.32 pN/nm
Rest Stalk Length	L_K	110 nm
Step size	d_K	8 nm
Stall $_F$orce	F_s^K	5.00 pN
Detachment Force	F_d^K	4.00 pN
Rate of attachment	π^K	5 s^{-1}
Rate of detachment at zero load	ϵ_o^K	1 s^{-1}

2. *In-vitro* Cytoplasmic Dynein Parameters

Parameter	**Symbol**	**Magnitude**
Arrhenius Constant	A^D	1.68497E39 nms^{-1}
Critical Temperature	T_C^D	286.1722 K
Activation Energy for $T<T_C^D$	E_a^{D1}	201.3638 kJ/mol
Activation Energy for $T\geq T_C^D$	E_a^{D2}	60.9441 kJ/mol
Spring Constant	k_D	0.32 pN/nm
Rest Stalk Length	L_D	50 nm
Step size	d_D	8 nm
Stall Force	F_s^D	1.25 pN
Detachment Force	F_d^D	0.87 pN
Rate of attachment	π^D	5 s^{-1}
Rate of detachment at zero load	ϵ_o^D	1 s^{-1}

3. *In-vivo* Kinesin-1 Parameters

Parameter	**Symbol**	**Magnitude**
Arrhenius Constant	A^K	1.72448E14 nms^{-1}
Activation Energy	E_a^K	65.05869 kJ/mol
Spring Constant	k^K	0.32 pN/nm
Rest Stalk Length	L_K	110 nm
Step size	d_K	8 nm
Stall Force	F_s^K	2.50 pN
Detachment Force	F_d^K	2.00 pN
Rate of attachment	π^K	5 s^{-1}
Rate of detachment at zero load	ϵ_o^K	1 s^{-1}

4. *In-vivo* Cytoplasmic Dynein Parameters

Parameter	**Symbol**	**Magnitude**
Arrhenius Constant	A^D	1.68497E39 nms^{-1}
Critical Temperature	To	286.1722 K
Activation Energy for T<To	E_a^{D1}	201.3638 kJ/mol
Activation Energy for T≥To	E_a^{D2}	60.9441 kJ/mol
Spring Constant	k_D	0.32 pN/nm
Rest Stalk Length	L_D	50 nm
Step size	d_D	8 nm
Stall Force	F_s^D	2.50 pN
Detachment Force	F_d^D	1.74 pN
Rate of attachment	π^D	5 s^{-1}
Rate of detachment at zero load	ϵ_o^D	1 s^{-1}

- **References**

1. Kunwar A., Tripathy S.K., Xu J., Mattson M.K., Anand P., Sigua R., Vershinin M., McKenney R., Yu C.C., Mogilner A. and Gross S.P. (2011) Mechanical Stochastic Tug-of-War Models cannot explain Bidirectional Lipid-droplet Transport: *PNAS 108:*18960-18965.

2. Kunwar A., Vershinin M., Xu J. and Gross S.P. (2008) Stepping, Strain-Gating andan Unexpected Force-Velocity curvefor Multiple-Motor-Based Transport: *Current Biology 18:*1173-1183.

3. Schnitzer M.J., Visscher K., Block S.M. (2000) Force production by single kinesin motors. *Nat Cell Biol.* 2:718–723.

4. Andreasson J.O.L., Milic B., Chen G.Y., Guydosh N., Hancock W.O., Block S.M. (2015) Examining kinesin processivity within a general gating framework: eLife 2015:e07403.